Ocean Engineering 131 (2017) 80–94

Contents lists available at ScienceDirect

Ocean Engineering

journal homepage: www.elsevier.com/locate/oceaneng

Evaluation of full scale shear performance of tension anchor foundations: Load displacement curves and failure criteria

Paolo Bergamo[a,1], Shane Donohue[a,*], Damian Callan[b], Adam Holland[b,2], John McCarey[b], William Brown[b,3], Michael McSherry[b], Cillian Ward[b], Giuseppina Amato[a], V. Sivakumar[a]

[a] School of Natural and Built Environment, Queen's University Belfast, Stranmillis Road, BT95AG Belfast, Northern Ireland, UK
[b] McLaughlin and Harvey Ltd., 15 Trench Rd, Newtownabbey BT36 4TY, Northern Ireland, UK

ARTICLE INFO

Keywords:
Post-tensioned anchor
Offshore foundation
Marine energy
Shear performance
Direct shear test
Full-scale testing

ABSTRACT

One of the biggest challenges faced by the offshore wave and tidal energy industry is the high cost of constructing and installing offshore foundations. Foundations based on post tensioned pile anchors can be effectively proposed to tackle this issue. A series of full-scale direct shear tests were performed on-shore to evaluate the shear resistance of post-tensioned pile anchor foundations designed for securing tidal turbine devices to a rock seabed. We focused, in particular, on the primary shear resistance mechanism of post-tensioned anchors, by applying a vertical force which mobilizes, a frictional force able to resist horizontal thrusts. Different load paths, involving monotonic or cyclic loading, were applied; several configurations for the footing of the foundation were tested. The footing stress-displacement behavior and the stress conditions at sliding failure from a number of different testing configurations were compared and analyzed. A marked consistency with the shear performance of natural rock joints was identified. This allows the behavior of tension pile foundations subjected to substantial horizontal loads to be modeled using relationships developed for rock joints, widely available in the literature. Additionally, the results obtained from different tests were also collated considering the various configurations adopted for the foundation-rock system and the applied load paths, to identify the factors that affect the shear resistance of the foundation.

1. Introduction

Among the most promising sources of renewable energy, the harvesting of electrical power from wind turbines or wave/tidal power generators, is a key resource in the area of the British Isles, because of the vast potential of offshore energy reserves (UK Government, 2003; DETINI, 2009; Renewable UK, 2013; EMEC, 2016). In this context, a critical problem currently encountered by civil engineering is the realization of adequate foundation systems for wind/wave/stream offshore turbine devices. These foundations must be capable of connecting these structures to the seabed and of transferring the loads applied to the turbines safely to the ground (e.g. Adhikari and Bhattacharya, 2011; Bhattacharya et al., 2012; Abhinav and Saha, 2015). These demanding engineering tasks significantly affect the installation costs of such turbines and may constitute up to 35% of the installed cost (Byrne and Houlsby, 2003). This influences negatively the cost competitiveness per megawatt when compared to energy from fossil fuels (DETINI, 2009).

Over recent years, several foundation solutions for tidal power generators have been developed and implemented. The most common solutions, that have been used for a range of different environments (e.g. water depth, nature of seabed), are: gravity foundations (e.g. McLaughlin and Harvey, 2016), piled foundations (e.g. Whittaker et al., 2007; Spagnoli et al., 2013), moored foundation solutions (Jeffcoate et al., 2015; Scotrenewables, 2016;), tripods with buckets and suction buckets. The advantages and disadvantages of each of these systems have previously been established (IEA – RETD, 2012). Considering the need to meet challenging engineering requirements and to reduce construction and deployment costs, the offshore foundation industry is continuously evolving, with new or hybrid solutions being developed. Recently, the use of foundations for tidal turbines based on post-tensioned anchors has been proposed, jointly with a system for their efficient installation in offshore environments (Callan et al., 2012). This foundation type aims to provide the tidal turbine

* Corresponding author.
E-mail address: s.donohue@qub.ac.uk (S. Donohue).
[1] Present address: Schweizer. Erdbebendienst, ETH Zurich, Sonneggstrasse 5, 8092 Zurich, Switzerland.
[2] Present address: Fast Engineering Ltd, 5 Windmill Court, Antrim BT41 2TX, Northern Ireland, UK.
[3] Present address: Gavin & Doherty Geosolutions Engineering UK Ltd, 7 Donegall Square West, Belfast BT1 6JH, Northern Ireland, UK.

http://dx.doi.org/10.1016/j.oceaneng.2016.12.033
Received 1 September 2016; Received in revised form 21 December 2016; Accepted 31 December 2016

Nomenclature

A	area
a	asperity angle
c_O	cohesion intercept
d_h	shear, horizontal displacement
d_v	normal, vertical displacement
d_{vj}	vertical displacement related to the closure of the rock joint and failure of asperities (net deformation or closure)
d_{vr}	portion of vertical displacement due to solid rock compression
d_{vt}	total vertical displacement
f_h	shear, horizontal force
f_{ha}	horizontal asymptotic load of the f_h–d_h curve
f_v	normal, vertical force
φ_b	basic friction angle
K_j	stiffness number
K_{nji}	initial normal stiffness for rock joint closure or failure
K_{nri}	initial normal stiffness of solid rock compression
k_{si}	initial shear stiffness referred to the f_h–d_h curve
K_{si}	initial shear stiffness referred to the τ–d_h curve
n_j	stiffness exponent
R_f	failure ratio
σ_n	normal, vertical stress
σ_{na}	horizontal asymptote of the σ_n–d_{vr} curve
τ	shear stress
τ_a	horizontal asymptotic of the τ–d_h curve
τ_{max}	shear stress at failure
V_m	maximum achievable closure for a rock joint

with sufficient bearing resistance, whilst at the same time reducing the overall size of the foundation when compared to gravity based foundations (thereby reducing concrete requirements). This system consists of small-diameter hollow bars drilled in the rocky seabed and secured to the underlying rock volume by means of grout bond. When tensioned using hydraulic jacks, they apply a vertical force on the underwater structure that replicates the self-weight of a ballasted structure to ensure its stability (Fig. 1). The technology of post tensioned anchors (hereafter referred to as "tension anchors") is readily available and widely used for a range of onshore applications (e.g. as micropiles for foundations and anchorages, soil nails for reinforcing soil, slopes or tunnels; see for instance standards BS EN 14490, 2010, and BS EN 14199, 2015, within Eurocode 7, 1997). Conversely, the use of tension anchors in underwater applications is less common, because of the difficulties in tensioning the anchors in the subsea environment, where access and operating conditions might be extremely difficult; hence these topics are currently the subject of industry research and development (Callan et al., 2012; Meggitt et al., 2013; Tiwari et al., 2014). Additionally, underwater structures may be subjected to substantial horizontal loads, e.g. generated by tidal currents (de Jesus Henriques et al., 2014) or induced by wave action, that the foundations are required to resist. Studies found in the literature that discuss the performance of piles or anchors embedded in rock mainly focus on the evaluation of their shaft resistance (see for instance Gu and Haberfield, 2004; Serrano and Olalla, 2004, 2006) rather than on their behavior when subjected to significant shear forces.

To assess the potential of tension anchor foundations to resist significant horizontal loads, as typically found in a tidal environment, a set of full scale, direct shear tests were conducted. These tests were performed onshore, on a particular foundation primarily designed to fix tidal stream turbines to a rock seabed (Callan et al., 2012), constituted by a circular footing connected to the bedrock by means of a post-tensioned anchor. These trials are part of a wider experimental phase aimed at testing the performance of this foundation system prior to offshore installation in its planned working environment (i.e. a shallow sea, with a depth of few tens of meters, with substantial tidal currents). In the experiments presented in this paper, the tension anchor foundation supports a specifically designed test rig through which normal and shear loads are applied to the foundation (Figs. 2 and 3). This experimental apparatus was installed in a schist quarry (Ballykinler, Co. Down, Northern Ireland) in order to test the tension anchor system on a weathered, poor quality rock. Additional tests on other imported rock types were also carried out (e.g. sandstone, gritsone or granite rock, concrete). Several configurations for the footing of the foundation were adopted. Different loading scenarios were applied during the tests, including (1) monotonic loading until the peak shear strength was mobilized, and (2) bidirectional cyclic shear loading until failure. The resultant shear and normal displacements were measured at the foundation footing by means of linear variable differential transformer (LVDT) sensors.

In both the experimental and subsequent analysis phases, attention was focused on the primary shear loading resistance mechanism of post-tensioned anchors, by applying a vertical force which mobilizes a frictional force able to resist horizontal thrusts (Fig. 1). Indeed, the anchor itself also opposes horizontal movements; however, this mechanism comes into play at large displacements, when the rock-foundation footing coupling has already failed, and the anchor provides the residual shear resistance. The evaluation of the resistance provided by the anchor is, however, not within the scope of this work. Therefore, testing and analyses was focused on relatively small displacements, and failure was considered to occur when the foundation footing-rock adhesion fails, so that the footing "slides" on the rock surface, save for the constraint later posed by the anchor.

The experimental apparatus and details of the tests are described in "Experimental method" (Sections 2.1 and 2.2). The acquired datasets were studied and interpreted with reference to the scientific literature concerning the shear behavior of natural rock joints (Section 2.3). In this area of study, a wide range of works have focused:

i) on the analysis of load-displacement relations for rock discontinuities prior to failure (e.g. Kuhlawy, 1975; Hungr and Coates, 1978; Kulhawy, 1978; Bandis, 1980; Bandis et al., 1983);
ii) on the definition of criteria representing the state of stress at failure for rock discontinuities (e.g. Patton, 1966; Jaeger, 1971; Barton, 1973; Hoek and Brown, 1980).

For both aspects, the behavior displayed by the foundation footing-

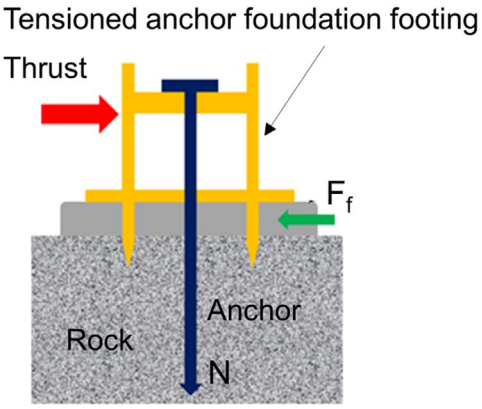

Fig. 1. Sketch of tension anchor foundation system. When the anchor is tensioned, a vertical force N (composed of tension in the anchor and self-weight) is applied to the structure to be secured. Consequently a friction force F_f is mobilized, which enables the structure to resist horizontal thrusts.

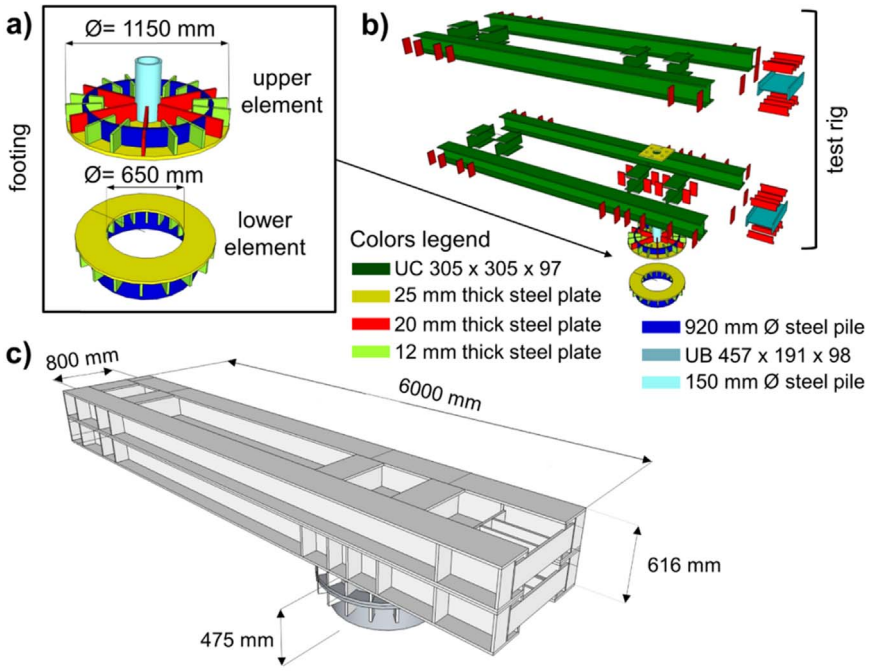

Fig. 2. Experimental apparatus, foundation footing and test rig. a and b) Exploded view of the elements composing the foundation footing and shear testing rig. c) Overall view of test rig and foundation footing, with key dimensions indicated.

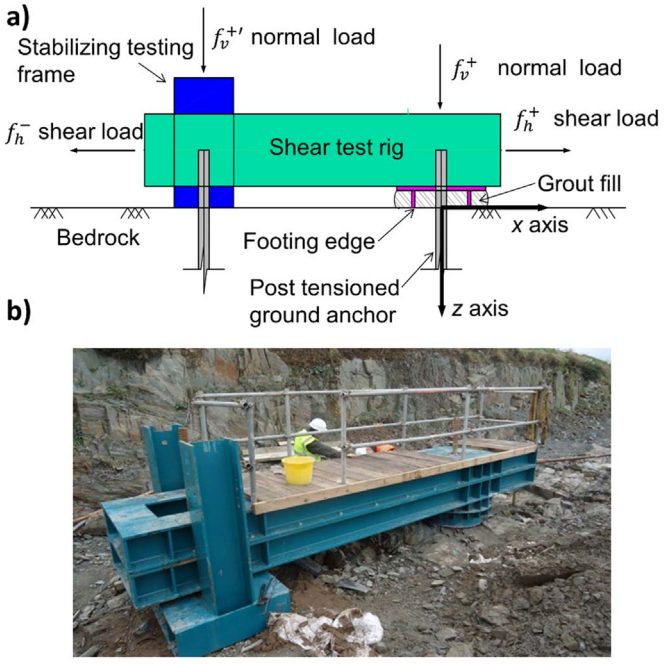

Fig. 3. Experimental apparatus. a) Sketch of the shear testing rig when installed on site, representing also the applied loads and the adopted spatial reference system. f_h and f_v identify shear and normal forces, respectively. Superscript $^+$ and $^-$ indicate the sign (positive or negative) of the applied loads according to the adopted sign convention. b) picture of the test rig system.

rock system in the tests carried out showed an appreciable degree of consistency with the response described and modeled for natural rock joints in literature. This allows the relationships developed for rock joints, widely considered in the literature, to be used for modeling the performance of tension anchor foundations subjected to substantial horizontal loads. The results obtained from different tests were also analyzed considering the various configurations adopted for the foundation-rock system and the applied load paths, to identify the factors that affect the shear resistance of the foundation ("Results and Discussion", Section 3).

2. Experimental method

2.1. Experimental apparatus

The foundation tested in this study is a post-tensioned anchor foundation (Callan et al., 2012). This is constituted by a ground anchor embedded in the rock mass, tensioned to exert a downward normal force on the foundation footing, which is a circular steel frame placed on top of the rock surface (Fig. 1). The rock anchor is a titan threaded hollow bar, 73/53 mm diameter (Ischebeck Titan, 2016).

The tested foundation was installed at different locations in the outcropping schist bedrock (unconfined compressive strength, UCS=39 MPa, rock-quality designation, RQD=40–50%) of a quarry in Ballykinler, Northern Ireland. The adopted installation followed manufacturer's recommendations (Ischebeck Titan, 2016): the anchor was installed in the rock mass with a sacrificial drill bit, using a rotary percussive drilling technique and a weak cement grout as flushing medium, pumped through the hollow center of the anchor. A maximum boring depth of approximately 6 m was reached. Towards the end of the drilling phase, a 0.4 water/cement ratio grout was injected, as recommended by the anchor manufacturer (Ischebeck Titan, 2016). This grout displaced the weaker flushing medium and, when cured, it formed a bond around the lower portion of the anchor and the rock mass. A free anchor length of 4 m was achieved by de-bonding the upper section of the anchor bar, this included the section of the anchor within the foundation. Once the anchor was installed, its upper portion, emerging from the rock mass for 2 m, was encapsulated in the foundation footing (Fig. 2a). The footing was constituted by two circular steel elements (Fig. 2a), bolted on top of each other. The lower element, the one in contact with the rock, is comprised of a steel tubular section, 300 mm long (in dark blue in Fig. 2a), with an inner and outer diameter of 880 and 920 mm, respectively. The lower edge of the tubular pipe was shaped in two alternative configurations: in one case, the edge was beveled with a bevel angle (β) of 45°; alternatively, the profile of the edge was flat (β=90°). It should be noted that the anchor, although sheathed in the foundation footing, was not coupled

with it, i.e. the anchor was not in direct contact with any of the elements of the shear foot. The system is described in detail by Callan et al. (2012).

The foundation footing was in turn housed into a bespoke designed and assembled shear testing rig (Figs. 2b, c), whose function was to transfer the externally applied loads to the footing. The test rig was an elongated fabricated steel frame composed by four 6 m long 305 UC 97 steel beams, arranged into two layers, the two sides of the rig being connected by means of transversal steel members. Fig. 2c shows an overall design of the testing rig and the foundation footing. When put in place, the rig rested, at one of its extremities, on the foundation footing; the other end was enclosed and supported by a stabilizing frame also composed of steel elements (Fig. 3a). This frame was required to prevent any rotational movement of the footing and to ensure that the applied load was a purely horizontal load and not a rotational one. Lubricated steel "knife edge" bearing pads were used to prevent up lift while reducing friction within the system. The stabilizing frame supported the underside of the rig on a slip bearing so that horizontal load was resisted entirely by the interaction of the footing and foundation rock. Fig. 3a and b shows a sketch and a picture of the test rig setup on site.

After the whole system (foundation and shear testing rig) had been installed, the ground anchor was tensioned by means of four hydraulic jacks, placed on the upper surface of the rig. The applied tension (f_v^+ in Fig. 3a) was progressively increased to the desired level of force, comprised within 490–1470 kN (50–150 t) depending on the different tests (see Section 2.2). A similar system, based on hydraulic jacks, was simultaneously used to apply a vertical force on the rig at the location of the stabilizing frame ($f_v^{+\prime}$ in Fig. 3a), to prevent an excessively asymmetrical loading of the testing rig, hence resisting the overturning moment induced by horizontal loads. In this case, the applied force was set to 441 kN (45 t) in all tests. Once the normal loads had been brought into operation, horizontal shear forces (f_h in Fig. 3a) were applied on the testing rig frame using tensioning bars connecting both ends to anchor blocks. Shear loads were applied either in a single direction, or alternately in both directions, depending on the desired loading path. The displacements produced at the base of the foundation footing, in the horizontal and, for some tests, vertical direction, were measured by means of LVDT's.

2.2. Experimental testing

A total of fourteen different tests were conducted using the experimental apparatus described above. Each test, numbered from 1 to 14, was characterized by a specific installation of the ground anchor, preparation and deployment of the foundation footing and loading path. In experiments including two or more successive loading phases, these are labeled with alphabet letters. Table 1 and Table 2 present a summary of the whole experimental work. See Tables A1–A4, in Appendix A, for a separate description of all tests. We illustrate here the different experimental conditions adopted for each test.

2.2.1. Installation of the ground anchor

As described in Section 2.1, the first step in the execution of the tests was the installation of the ground anchor, which was drilled into the rock mass. Three different experimental setups were investigated:

i) The anchor was drilled into the schist constituting the natural outcropping bedrock at the test site of Ballykinler quarry (Fig. 4a). Different locations were chosen in the quarry, so that the foundation was installed on either a relatively competent or a weathered schist. As summarized in Table 2, in tests 1, 6, 7, 8, 9, 10, 14 the foundation footing was directly placed on the schist bedrock.
ii) Before drilling the anchor in the bedrock, a cylindrical hole, ~0.4 m deep and with a diameter of ~1 m, was excavated into the schist rock. The anchor was then driven into the underlying rock volume, which was subsequently backfilled with 40 MPa concrete (standard EN 206-1:2000; European Committee for Standardization, 2000). The concrete was then left to cure for 10 days (period between the installation of the experimental setup and the test execution); it thus formed a compact slab, encased in the bedrock mass and with a smooth upper surface, enclosing the upper segment of the buried portion of the anchor (Fig. 4b). This preparation technique was adopted for tests 2, 3, 4, 5 (Table 2). For these tests, the foundation footing was hence placed on the smooth surface of a concrete slab.
iii) Before drilling the anchor in the bedrock, a trench was excavated in the schist bedrock. A boulder of a different rock type was then housed in the trench and coupled with the surrounding schist mass by adding 40 MPa concrete (standard EN 206-1:2000; European Committee for Standardization, 2000). Here again, the concrete curing time corresponded to the period between the installation of the anchor and the shear test execution (10 days). Finally, the anchor was drilled into this two-layer rock mass, where the lower layer was constituted by the schist bedrock and the upper layer was the encased rockboulder it (Fig. 4c). Three different types of rock were used: red sandstone (test 11), Mourne granite (test 12), and gritstone (test 13, Table 2). This preparation technique enabled the foundation performance to be evaluated on better quality, smoother rock materials, when compared to the original schist bedrock of the test site.

2.2.2. Foundation footing preparation

The second step in the execution of the tests was the preparation and deployment of the foundation footing (see Section 2.1 and Fig. 2a, b). Here again, three different alternatives were adopted in the tests:

i) The foundation footing was directly placed on the rock or concrete slab, its lower edge in direct contact with the underlying material. No grout layer (see below) was added between the shear foot and the rock. This configuration was implemented for tests 1, 2, 3 (*Naked steel frame* in Table 2).
ii) Before the footing was housed in the testing rig, its inner volume was filled with grout and left to cure for 7 days. As a result, the footing face in contact with the underlying rock or concrete slab was a smooth flat surface, with an area A=0.665 m^2 (Fig. 4d). Tests 4 and 6 were conducted using this footing configuration (Grouted footing in Table 2).
iii) The inner volume of the footing was filled with grout when the footing had been already put in place, and left to cure for approximately 14 days. The grout created a layer adhering to both the steel frame of the footing and the underlying rock or concrete surface (Figs. 4e, f). Care was taken to avoid direct contact between the anchor and the grout layer; the anchor bar was protected from contact with the grout using a closed cell foam (polystyrene) insulation to allow movement of the shear foot without generating any shear resistance from the anchor bar. This procedure was

Table 1
Maximum normal load applied before the start of the shear loading phase (f_{v0}), expressed in kN and t.

Tests	Normal load at the start of shear loading phase (f_{v0})	
	(kN)	(t)
2a, 3a, 4a, 5a, 5b	490	50
1a	883	90
2b, 3b, 4b, 5c	981	100
1b	1177	120
8	1422	145
1c, 2c, 3c. 4c, 5d, 6, 7, 9a, 9b, 10a, 10b, 10c, 11a, 11b, 11c, 12a, 12b, 13a, 13b, 13c, 14a, 14b, 14c	1471	150

Table 2
Table presenting the arrangement of the foundation-rock system and adopted shear loading path. The bevel angle (β) of the footing edge is 45°, unless differently specified.

	Material underlying the foundation footing								
	Concrete slab			Schist bedrock			Sandstone slab	Granite slab	Gritstone slab
	Configuration of foundation footing								
Shear loading path	Naked steel frame	Grouted footing	Footing grouted in place	Naked steel frame	Grouted footing	Footing grouted in place	Footing grouted in place	Footing grouted in place	Footing grouted in place
Monotonic, unidirectional increment of f_h to failure	2a (β=90°), 2b (β=90°), 2c (β=90°), 3a, 3b, 3c	4a, 4b, 4c, 5b, 5c, 5d	5a	1a (β=90°), 1b (β=90°), 1c (β=90°)		7 (β=90°), 8, 9b (β=90°) 9a (5, β=90°)			
Unidirectional cycles. Max. f_h490 kN. (no. of cycles)					6 (9)				
Bidirectional cycles. Max. $\|f_h\|$=490 kN. (no. of cycles)						14a (48)			
Bidirectional cycles. Max. $\|f_h\|$=735 kN. (no. of cycles)						10a (5) 14b (46)	11a (5)	12a (5)	13a (5)
Bidirectional cycles. Max. $\|f_h\|$=981 kN. (no. of cycles)						10b (3)	11a (2)	12b (2)	13b (2)
Bidirectional cycles to failure. Max. $\|f_h\|$ > 981 kN. (no. of cycles)						10c (3 – no failure) 14c (8)	11c (4)		13c (4)

followed in tests 5a, 7, 8, 9, 10, 11, 12, 13, 14 (*Footing grouted in place* in Table 2). A partial exception was constituted by tests 5b-d. After reaching sliding failure at the end of experiment 5a (involving the failure of the grout-concrete slab bond, thus producing a rugged contact surface), the subsequent tests (5b-d) were executed by repositioning the shear foot in its original place (interlocking the grout asperities), without restoring the grout bond.

2.2.3. Loading path

After the foundation was completely installed and connected to the testing rig, vertical and horizontal forces were applied as described in section Section 2.1, following the desired loading path. First, a normal force (f_v) was progressively applied on the test rig above the foundation by tensioning the ground anchor with hydraulic jacks (Fig. 3a). The normal force was increased up to the desired level (f_{v0}, comprised between 490 and 1470 kN, i.e. 50–150 t, depending on the different tests), which was then intended to be kept constant in the following phase of shear loading. See Table 1 for a complete list of the values of f_{v0} adopted in all tests. Figs. 5a and b show a typical increment of vertical force from 0 kN to the desired maximum value of 1471 kN, as well as the produced resultant vertical displacements (d_v) measured at the base of the foundation footing (initial phase of test 14a).

Once the preset level of f_v has been reached, the following phase of application of shear loads (f_h) was initiated. A variety of different loading-unloading paths, with increasing levels of complexity, was followed in the various tests:

i) Monotonically increasing the horizontal force, applied in a single direction, until the condition of sliding failure at the base of the foundation footing was achieved. The shear force was progressively increased in 98 kN steps, with a 1 min interval between successive load increments. When failure was considered imminent, the load increments decreased to 49 kN (5 t) steps. The condition of sliding failure was characterized by a sudden and sharp increase of horizontal displacement measured at the footing (d_h), in response to a stable increase of applied shear load f_h; the subsequent release of f_h showed the predominance of unrecoverable, permanent sets (see Fig. 5c showing a typical load-displacement graph from a test involving a monotonic increase of f_h to failure, test 5c). Overall, tests 1, 2, 3, 4, 5, 7, 8, 9b implemented this loading path.
ii) Repeated unidirectional loading-unloading cycles. Each cycle involved increasing f_h to a maximum value (490 kN, 50 t), again through 98 kN steps separated by 1 min intervals. The loading phase was then followed by a reduction to 0 kN, completed in a single step. Tests 6 and 9a (Fig. 6a, b) implement this loading path.
iii) Repeated bidirectional loading-unloading cycles. Each cycle was comprised of alternating load-unload paths in the positive and negative direction (see Fig. 3a for sign reference), reaching the same absolute value for the maximum applied load in either direction (see Figs. 6c, d for an example from test 14a). Regarding the loading pattern, the horizontal force was progressively raised and decreased, through successive steps (49–98 kN steps, tests 10–13) or a continuous increase/decrease (test 14, Fig. 6c, d). The average duration per full cycle was 3.5 min for the tests where $|f_h|_{max}$=490 kN (test 14a); 6.1 min for the tests with $|f_h|_{max}$=735 kN (tests 10a, 11a, 12a, 13a, 14b); 8.2 min for the tests where $|f_h|_{max}$=981 kN (tests 10b, 11b, 12b, 13b). The final phases of tests 11, 13 and 14, involved cyclic amplitudes $|f_h|$ > 981 kN, which resulted in sliding failure.

The different shear loading paths described above (monotonically increasing, unidirectional or bidirectional cycles) were also combined within the same test, in a succession of various loading phases (labeled with letters, see Tables 1 and 2).

As shown by Figs. 6a and c, the phase of application of shear loads is characterized by a gradual, limited decrease in the value of f_v

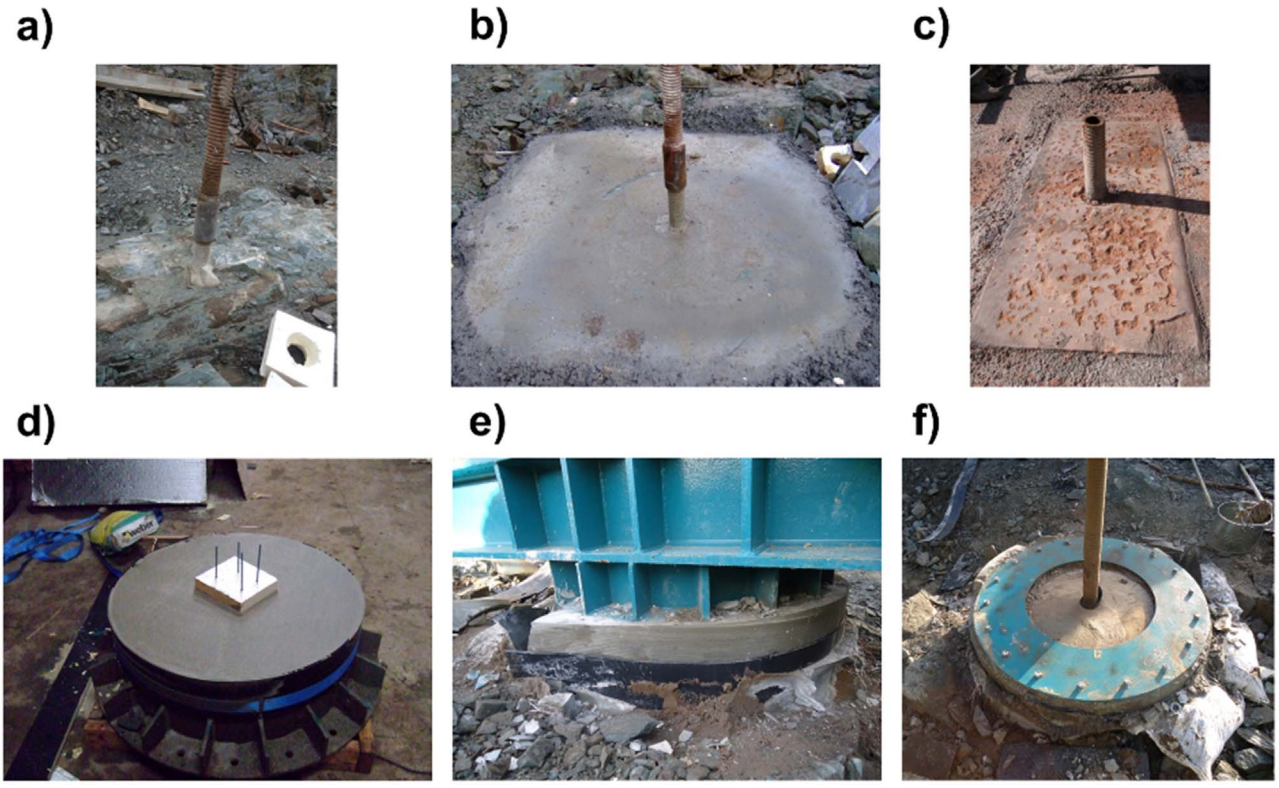

Fig. 4. Different alternatives for the installation of ground anchor and the configuration of the foundation footing. Panels a-c: installation of ground anchor. a) Ground anchor drilled in schist bedrock. b) Anchor surrounded by a concrete slab. c) Anchor drilled into a two layer rock formation, the upper layer being constituted by a block of red sandstone (visible in the picture), resting on schist bedrock. Panels d-f: configuration of foundation footing. a) Footing filled with grout and left to cure before its placement on site. b) Footing and grout layer added when the footing was already in place. c) Lower element of the foundation footing and of grout layer cast in place. (For interpretation of the references to color in this figure legend, the reader is referred to the web version of this article.)

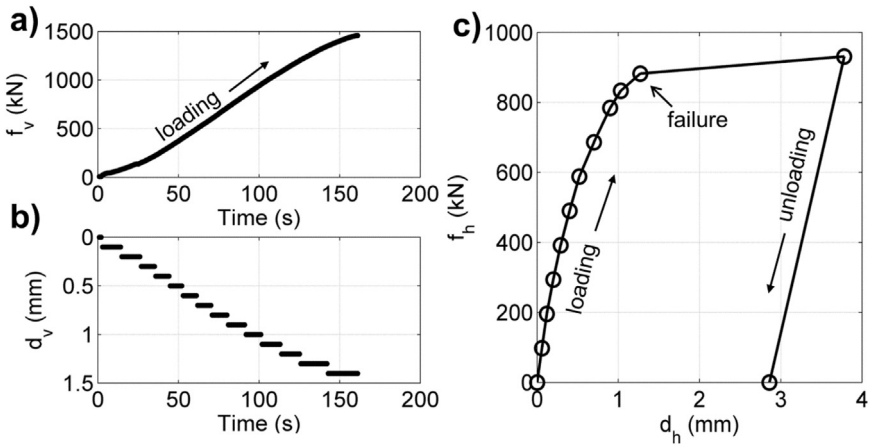

Fig. 5. Application of vertical and horizontal loads and produced displacements. a) and b) Typical initial loading phase of performed tests, where the normal force was gradually increased from 0 kN to the desired value of 1471 kN (a). In b) the vertical displacements measured in this phase are shown (a and b refer to test 14a). c) Shear load-displacement graph in a typical test (test 5c) involving the unidirectional and monotonic increment of f_h until sliding failure is reached. The following unloading path shows the prevalence of permanent sets.

(applied normal force ensured by the hydraulic jacks tensioning the anchor). This decrease is due to i) the loss of fluid through jack gaskets (particularly evident in the initial phase of shear loading) and ii) the extension of jack cylinders made possible by the increasing vertical (downward) displacements of the foundation footing during the shear loading phase. The loss of pressure in the jacks exerting the normal load f_v is limited, amounting to 10% and 12% in the two most extended tests (test 14a and 14b), involving 48 and 46 cycles of bidirectional shear loading, respectively.

Table 1 and Table 2 present an overall summary of the whole experimental work, describing how the different possible configurations for the foundation footing-rock system and the various loading paths, illustrated above, were combined in a series of tests aimed at evaluating the performance of post tensioned anchor foundations in a variety of different conditions. Each test (numbered from 1 to 14), was characterized by a specific installation procedure leading to a particular configuration for the foundation-rock system; the corresponding loading paths, if constituted by two or more phases, are designated with a letter. See Tables A1–A4, in Appendix A, for a separate description of all tests.

2.3. Relevant aspects of mechanical behavior of natural rock joints

This Section introduces relevant aspects of the mechanical behavior

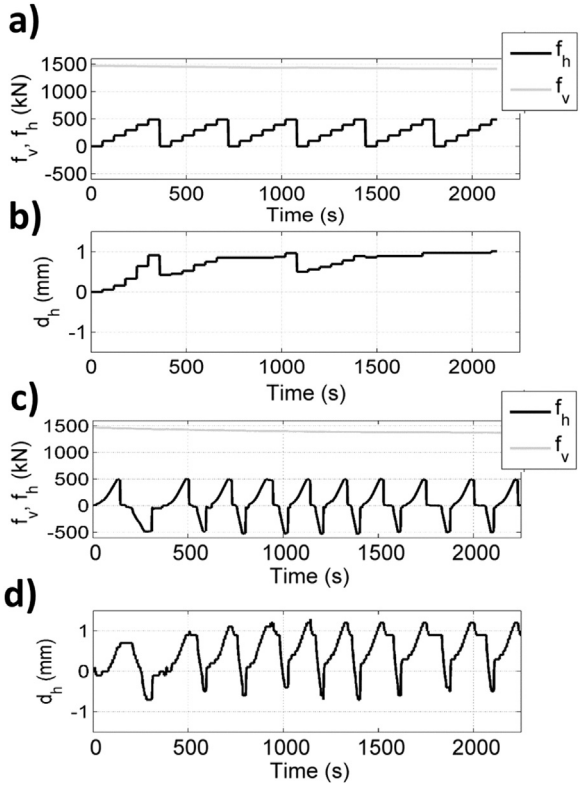

Fig. 6. Unidirectional (a, b) and bidirectional (c, d) cyclic loading paths. a) Applied normal and horizontal loads in a typical unidirectional cyclic loading test (test 9a). b) Measured horizontal displacements. c) Applied normal and horizontal loads in a typical bidirectional cyclic loading experiment (first 10 cycles from test 14a). d) Corresponding horizontal displacements.

of natural rock joints, which have been adopted to assist the interpretation of the shear test data produced in this study.

2.3.1. Load-displacement relationships

According to the work of Bandis et al. (1983), the total normal deformation (d_{vt}) measured in a rock joint subjected to normal stress is constituted by the sum of two components,

$$d_{vt} = d_{vr} + d_{vj} \tag{1}$$

where d_{vr} is the portion of vertical displacement due to solid rock compression, and d_{vj} is related to the closure of the rock joint and failure of asperities, and it is referred to as net deformation or closure. Bandis et al. (1983) observed that at the initial loading states, the total observed deformation (d_{vt}) is predominantly due to the displacements occurring across the joint interface (d_{vj}). Successively, under increasing values of normal load, the joint closely reaches its closed state, and any further increase in normal stress (σ_n) is taken up by the solid rock below and above the joint (therefore d_{vr} becomes dominant). According to Kulhawy (1975) and Bandis et al. (1983), the relationship between σ_n and d_{vr} may be expressed as a hyperbolic curve with downward concavity, i.e. tending towards a horizontal asymptote on the σ_n axis:

$$\sigma_n = \frac{d_{vr}}{\frac{1}{K_{nri}} + \frac{d_{vr}}{\sigma_{na}}} \tag{2}$$

where K_{nri} and σ_{na} are the initial tangent of the σ_n–d_{vr} curve (or initial normal stiffness of solid rock compression) and the horizontal asymptote to the same curve, respectively. To model the behavior of net deformation in rock joints (dv_j), Bandis et al. (1983) suggested the following equation, again a hyperbolic relation, but with an upward oriented concavity (i.e. tending towards a vertical asymptote on the d_{vj} axis):

$$\sigma_n = \frac{d_{vj}}{\frac{1}{K_{nji}} - \frac{K_{nji}}{V_m} d_{vj}} \tag{3}$$

where K_{nji} is the initial normal stiffness for joint closure or failure (K_{nji} being the ratio between the increase in applied normal stress and the increase in produced d_{vj} at $\sigma_n \to 0$), and V_m is the vertical asymptote to the hyperbola and it is the maximum achievable closure for the joint (.i.e. the condition where the joint asperities are perfectly interlocked or have failed).

In a similar fashion, experimental observations of the shear behavior of different types of rock joints and at different levels of normal stresses have led to the definition of hyperbolic form for shear load (f_h) – shear displacement (d_h) relationships (Kulhawy, 1978; Hungr and Coates, 1978; Bandis et al., 1983). In particular, Kulhawy (1978) has validly proposed and applied:

$$f_h = \frac{d_h}{\frac{1}{k_{si}} + \frac{d_h}{f_{ha}}} \tag{4}$$

where k_{si} is the initial shear stiffness (the ratio between the increase in applied load and the increase in resultant displacement at $f_h \to 0$) and f_{ha} is the horizontal asymptotic load of the f_h–d_h hyperbolic curve. These two parameters can be correlated to the quality of the coupling between the two faces of the rock joint. According to Kulhawy's (1978) and Bandis et al.'s (1983) experimental observations, fresh planar and weathered rock joints are characterized by lower values of k_{si} and by highly nonlinear f_h–d_h curves (i.e. by lower values of parameter f_{ha} in Eq. (4)). Vice versa well interlocked, unweathered joints yield steeper and more linear f_h–d_h relations (features corresponding to higher k_{si} and f_{ha}). Kulhawy (1978) and Bandis et al. (1983) have also investigated the influence of the applied normal stress on shear load – displacement relationships, proposing and validating the following equations:

$$\frac{k_{si}}{A} = K_{si} = K_j (\sigma_n)^{n_j} \tag{5}$$

$$\frac{f_{ha}}{A} = \tau_a = \frac{\tau_{max}}{R_f} \tag{6}$$

where A is the rock joint area (so that $K_{si}=k_{si}/A$ is the initial slope of the shear stress τ–d_h curve, and $\tau_a=f_{ha}/A$ is its horizontal asymptote), K_j=stiffness number, n_j=stiffness exponent, τ_{max}=shear stress at failure, which depends on σ_n according to the failure envelope (see Section 2.3.2). R_f, or failure ratio, expresses the ratio of the failure deviator stress to the deviator stress predicted by the hyperbola (Eq. (4)). R_f is ≤1 and it is related to the nonlinearity of the f_h–d_h curve; values close to 1 indicate a marked curvature of the hyperbola, while lower values correspond to a more linear appearance of the f_h–d_h relation.

2.3.2. Failure criterion

Several strength criteria, correlating the levels of shear and normal stress at failure, have been defined in the literature for rock masses (Patton, 1966; Jaeger, 1971; Barton, 1973; Hoek and Brown, 1980). Although their mathematical formulation may differ, all criteria envisage a failure envelope that, in a τ_{max} (peak shear stress) versus σ_n (normal stress) representation, is characterized by a steeper slope at

low values of σ_n and by a gentler slope at higher values of σ_n. The two different patterns are determined by the mechanisms controlling the shear resistance of the rock joints. At low values of σ_n, the shear resistance includes a component related to friction and a second component related to dilation. At higher σ_n the contribution of dilation becomes negligible, and friction and cohesion are the mechanisms controlling the shear resistance (Johnston and Lam, 1989; Roosta et al., 2006).

In agreement with these concepts, the shear strength criterion (Patton, 1966) defines a bi-linear envelope, expressed through the following equations:

$$\tau_{max} = \sigma_n tan(\varphi_b + \alpha) \text{for low normal stress} \quad (7)$$

$$\tau_{max} = c_0 + tan(\varphi_b) \text{for high normal stress} \quad (8)$$

where α is the asperity angle, φ_b is the basic friction angle and c_O is the cohesion intercept. The angle α is directly related to the dilatant behavior of rock joints under shear loading (Huang et al., 1993; Alejano and Alonso, 2005).

3. Results and discussion

3.1. Load-displacement relationships

3.1.1. Normal load – normal displacement relationship

All direct shear tests presented in this work were preceded by the gradual application of the vertical load (f_v; Section 2.2). Fig. 7 shows the σ_n (normal stress)–d_v curves recorded for the tests for which measurements of d_v are available (tests 10–14). Fig. 7a-d, refer to tests where the shear foot was placed on slabs of different rock types (sandstone, granite, gritstone) or on a fresh surface of schist bedrock. The measured d_v are modest (≤0.6 mm at $\sigma_{n\ max}$=2.21 MPa), and the σ_n–d_v relationships show a similar trend, defined by a curve with downward concavity. Following the consideration of Bandis et al. (1983), that the observed vertical displacements are partly due to solid

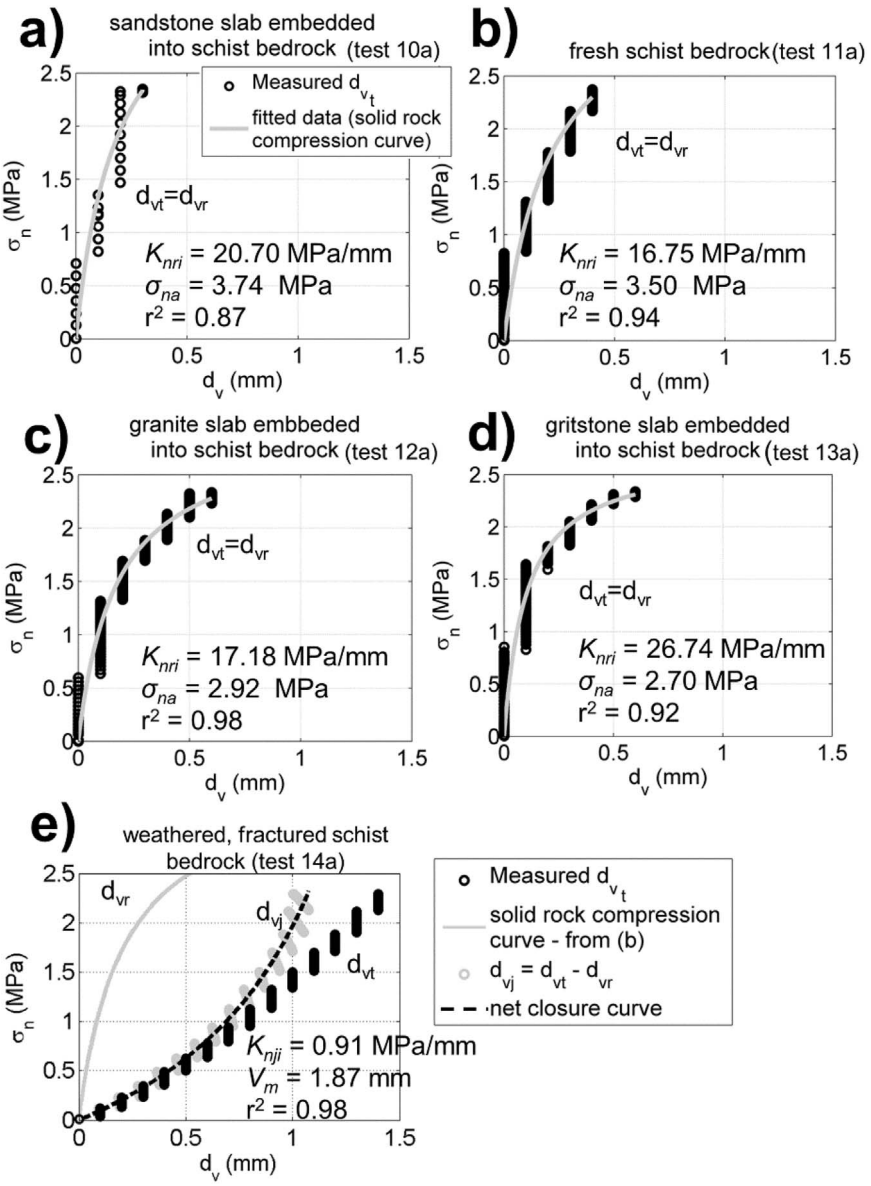

Fig. 7. Experimental σ_n–d_v curves obtained in the initial test phase of gradual application of normal load to the shear foot.

rock compression and partly to closure or failure of asperities (Eq. (1)), as the rock surfaces in contact with the shear foot were relatively smooth and flat, it was reasonably assumed that the contribution of asperity closure to the measured deformation was negligible. The observed d_v=d_{vt} was, therefore, considered to be purely related to solid rock compression (d_{vr}); hence these data were fitted with Eq. (2) (gray lines in Fig. 7). It is worth remarking that the experimental σ_n-d_{vr} curves observe the same trend defined by Kulhawy's (1975) and Bandis et al.'s (1983) model (Eq. (2)), that is a hyperbola tending towards a horizontal asymptote. The data fitting is good, expressed here and subsequently with the coefficient of determination, r^2. The values obtained for the constituent parameters of Eq. (2) (K_{nri} and σ_{na}) lie in relatively narrow intervals (16.75–26.74 MPa/mm and 2.70–3.74 MPa), suggesting similar behavior for the different configurations of the foundation footing in solid rock compression.

In Fig. 7e, which corresponds to a test where the shear foot was in contact with weathered schist bedrock, the observed σ_n–d_v relationship exhibits a different pattern (curve with upward concavity) and larger values of vertical displacement. Considering the state of the rock, in this case the contribution of joint closure (d_{vj}) could not be neglected, and therefore the measured d_v=d_{vt}=d_{vr}+d_{vj} (Eq. (1)). The d_{vr} component in Fig. 7e was reasonably modeled using the hyperbolic curve from Fig. 7b, which refers to a test on fresh schist); gray line in Fig. 7b, also reported in Fig. 7e). The ratio between d_{vt} and d_{vr} at σ_n=1 MPa in Fig. 7e is 8, within the range of 5–30 obtained by Bandis et al. (1983). Subtracting d_{vr} from the measured displacement d_{vt}, d_{vj} is obtained (Eq. (1), gray circles in Fig. 7e), the component related to the closure and/or failure of rock asperities. The obtained σ_n–d_{vj} graph was interpreted using the corresponding relationship from Bandis et al. (1983; Eq. (3)), which defines a hyperbolic function with an upward concavity; this is actually the shape of the experimental σ_n–d_{vj} curve in Fig. 7e. The fitting between Eq. (3) and the experimental data is excellent (r^2=0.98), and the resultant V_m and K_{ni} parameters are 1.87 mm and 0.91 MPa/mm, both comparable to values expected for rugged and weathered rock joints according to Bandis et al. (1983).

3.1.2. Shear load – shear displacement relationship

To investigate the shear load – shear displacement behavior in all tests for which horizontal measurements d_h are available (tests 2–6 and 8–14, Appendix A), the pre-peak shear load - shear displacement stage was considered from the experiments implementing a monotonic load to failure, or from the first loading path from cyclic tests (Table 2).

As shown in Fig. 8, the shear load -shear displacement curves from different tests consistently display non-linear behavior. This feature is in agreement with experimental observations on natural rock joints, for which hyperbolic functions were proposed (Kulhawy, 1978; Hungr and Coates, 1978; Bandis et al., 1983). The f_h–d_h function introduced by Kulhawy (1978; Eq. (4)) was applied to the experimental load – displacement curves and the best fitting values of k_{si} (initial shear stiffness) and f_{ha} (horizontal asymptote of the curve) were determined. As shown in Fig. 8, the agreement between the hyperbolic function of Eq. (4) and the experimental data is excellent. k_{si} and f_{ha}, parameters defining the shape of the f_h–d_h relationship, can be correlated to the quality of the coupling between the shear foot and the underlying rock or concrete surface. According to Kulhawy's (1978) and Bandis et al. (1983), planar and weathered rock joints are characterized by lower values of k_{si} and by highly nonlinear f_h–d_h curves (i.e. by lower values of parameter f_{ha}, Eq. (5)). By contrast, well interlocked, unweathered joints yield steeper, more linear f_h–d_h relationships (i.e. higher k_{si} and f_{ha}). Similar behavior can be traced in the load – displacement relationships shown in Fig. 8. Figs. 8b, c both compare the f_h–d_h curves for tests with the same applied normal stress and rock type, but in one case the shear foot was grouted in place, whereas in the other case the grout was left to cure before putting the footing in place. In both cases, the presence of the bond ensured by the grout cured in place resulted in a steeper and more linear f_h–d_h curve.

Fig. 9 displays the initial shear stiffness (k_{si}) and horizontal asymptote of the hyperbolic curve (f_{ha}) derived by fitting Eq. (4) to the experimental f_h–d_h curves from all considered tests. The quantitative characterization of experimental f_h–d_h curves through the estimation of parameters k_{si} and f_{ha} is of fundamental importance when evaluating the shear performance of tensioned anchor foundations; steeper f_h–d_h curves imply smaller displacements at the same level of shear loading (hence less sliding work degrading the foundation footing-rock coupling; Qiu and Plesha, 1991; Donohue and Bergamo, 2016). The following trends in the distributions of the k_{si},f_{ha} couples can be identified in Fig. 9:

i) All factors that contribute to make the shear foot-rock/concrete coupling firmer result in an increase of k_{si} and/or f_{ha}. In particular, a) when only the steel frame of the shear foot is in contact with the underlying concrete slab (red circles in Fig. 9), a 45° beveled edge (tests 3a,b,c), penetrating more easily into the concrete surface, yields higher k_{si} and f_{ha} as compared to a flat edge of the shear foot (tests 2a,b,c); b) an increase of the contact surface between the shear foot and rock/concrete via the filling of the foot steel frame with grout further improves the f_h–d_h curves (compare circles to dots); c) when the grout is cast in place, i.e. when the grout exerts a bond between the foot and the rock or concrete, a further increase

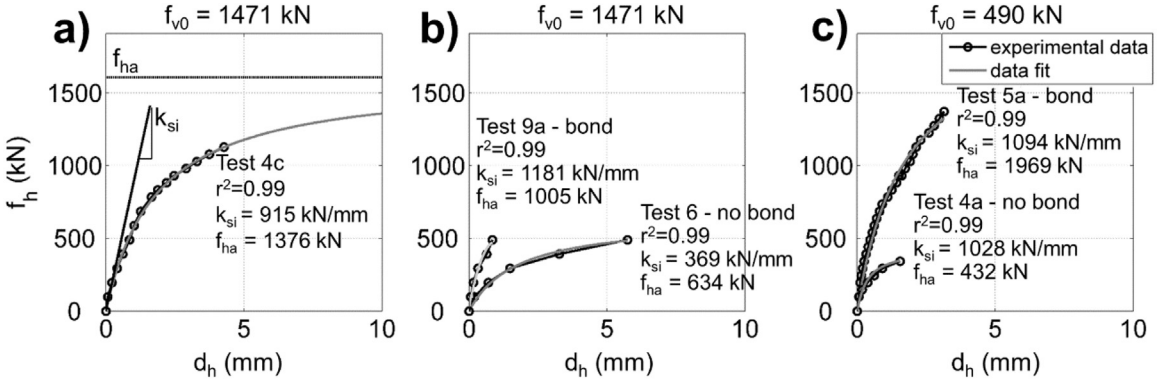

Fig. 8. Experimental f_h–d_h curves. a) f_h–d_h curve for a test involving the grouted shear foot superimposed to a concrete slab (test 4c), with f_{v0}=1471 kN. No bond between the shear foot and the concrete surface is present (footing not grouted in place). b) Comparison between f_h–d_h curves from two tests involving the grouted shear foot superimposed to a schist bedrock (tests 6 and 9a), with f_{v0}=1471 kN. In one case the shear foot was grouted in place (hence there is a bond between the foot and the schist bedrock). In the other case no bond is present (footing grouted separately). c) Comparison between pre-peak f_h–d_h curves from two tests involving the grouted shear foot superimposed to a concrete slab (tests 4a and 5a), with f_{v0}=490 kN. In one case the shear foot was grouted in place. In the other there is no bond.

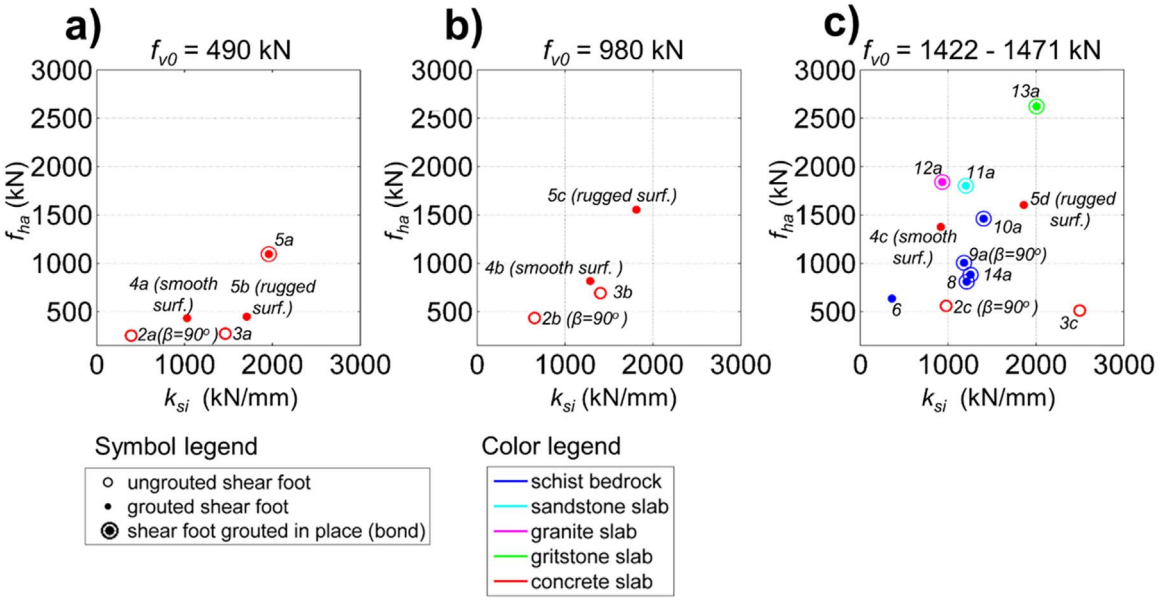

Fig. 9. Parameters k_{si} and f_{ha} of the hyperbolic relation f_h–d_h (Eq. (4)) obtained from the analyzed shear loading paths (pre-peak shear load - shear displacement stage from the experiments implementing a monotonic load to failure, or from the first loading path from cyclic tests). k_{si}, f_{ha} couples are subdivided in the three panels according to the value of normal load at the start of the shear loading path (f_{v0}). Labels refer the name of each test. The bevel angle is included in the labels when β=90° (otherwise β=45°). Labels with "smooth" or "rugged surface" allow to appreciate the different performance of tests 4a,b,c versus 5b,c,d, otherwise characterized by the same configuration of the footing-concrete system.

of the k_{si} and/or f_{ha} is produced (compare circled with plain dots in Fig. 9; see also Fig. 8b-c); d) when the shear foot is placed on compact materials (gritstone, sandstone, granite, concrete) it performs better (higher k_{si} and f_{ha}) when compared to fractured and weathered rock such as schist bedrock; e) the presence of interlocking asperities on the foot-rock/concrete contact area results in greater k_{si}, f_{ha} as opposed to smooth surfaces; (compare red dots marked with "smooth" versus "rugged surface" labels).

ii) Given the same shear foot-rock/concrete configuration, k_{si} and f_{ha} generally increase as the applied vertical load (f_{vo}) increases.

Feature (i) is in agreement with Kulhaway's (1978) and Bandis et al.'s (1983) observations, associating fractured and weathered rock joints to highly nonlinear f_h–d_h curves, and well interlocked, unweathered joints to steeper and more linear f_h–d_h relationships.

As for the dependence of shear load – displacement relationship on the applied normal load (ii, above), this trend is again in accordance with the findings of Kulhawy's (1978) and Bandis et al. (1983), expressed in Eqs. (4)–(6). We applied these relationships to the tests where shear loading paths were repeated at different levels of applied normal stress (tests 2, 3, 4, 5), to estimate the parameters K_j, n_j and R_f (Eqs. (5) and (6)), that describe the relationship between applied shear (τ=f_h/A), normal stresses (σ_n=f_v/A) and resultant horizontal displacements (d_h). Here again, the fitting between experimental and simulated τ-σ_n-d_h curves was good (Fig. 10). Obtained K_j, n_j lie at the lower range of values expected by Kulhawy (1978) and Bandis et al. (1983) from direct shear tests on rock discontinuities. Consistent with the outcome of the same tests, R_f are comprised within 0–1, with values close to 1 corresponding to highly nonlinear shear stress –displacement curves. Also, in agreement with Kulhawy's (1978) and Bandis et al.'s (1983) experimental observations, an improvement of the shear foot-concrete coupling (thanks to sharper edges of the foot steel frame in Fig. 10a-b, or thanks to interlocking asperities in Fig. 10c-d) results in an increase of K_j, n_j values and a decrement of R_f (i.e. steeper τ–d_h curves).

Overall, the relationships derived from the literature have been successfully applied to the load-displacement relationships observed from a tensioned anchor foundation placed on various types of rock and concrete. These relationships have proven to be adequate in representing (i) the normal load – normal displacement relation during the initial phase of gradual application of vertical load and (ii) the shear load – displacement curve in the subsequent stage of horizontal loading. This enabled changes in the shear load – displacement curves introduced by improvement of the foot-rock/concrete coupling to be quantified. Hence, these relationships can be proposed as a tool for the prediction of the response of tensioned anchor foundations under operational loads as the parameters appearing in the equations (Eqs. (2)–(6)) are related to the quality and geometry of the contacting materials.

3.2. Failure criterion

Figs. 11a and b display the values of maximum shear load ($f_{h\ max}$) and vertical load at the sliding failure of the shear footing. The couples of $f_{h,\ max}$, f_v show two different trends, one for the tests where a grout layer was added at the base of the foundation footing (Fig. 11a), and one for the tests where the steel frame of the footing was placed directly on the rock or concrete surface, without grout (Fig. 11b). For the first group of tests (Fig. 11a), the relationship between applied vertical load and peak shear load appears to be a directly proportional. This behavior suggests the prevalence of frictional and dilatant mechanisms in controlling the shear resistance of the foundation (Johnston and Lam, 1989; Roosta et al., 2006), and it is well approximated by Patton's (1966) formulation of failure criterion for rock joints at low values of normal stress (Eq. (7)). The slope for this linear failure envelope is 0.95, corresponding (Eq. (7)) to a sum of basic friction angle φ_b and asperity angle α equal to 44.2°, in good agreement with the value (45°) recovered by Hungr and Coates (1978) from direct shear tests on natural rock joints. The fit between Patton's (1966) linear envelope and the experimental data is good, with most of data points being comprised in a ± 25% interval. The only outlier is the failure condition from test 5a, where the foundation shear foot was grouted in place and superimposed to a concrete slab (circled red dot in Fig. 11a). In this case, the bond exerted by the grout on the regular surface of the concrete slab probably gave rise to a cohesive behavior that significantly increased the value of peak shear stress. Despite this, the general

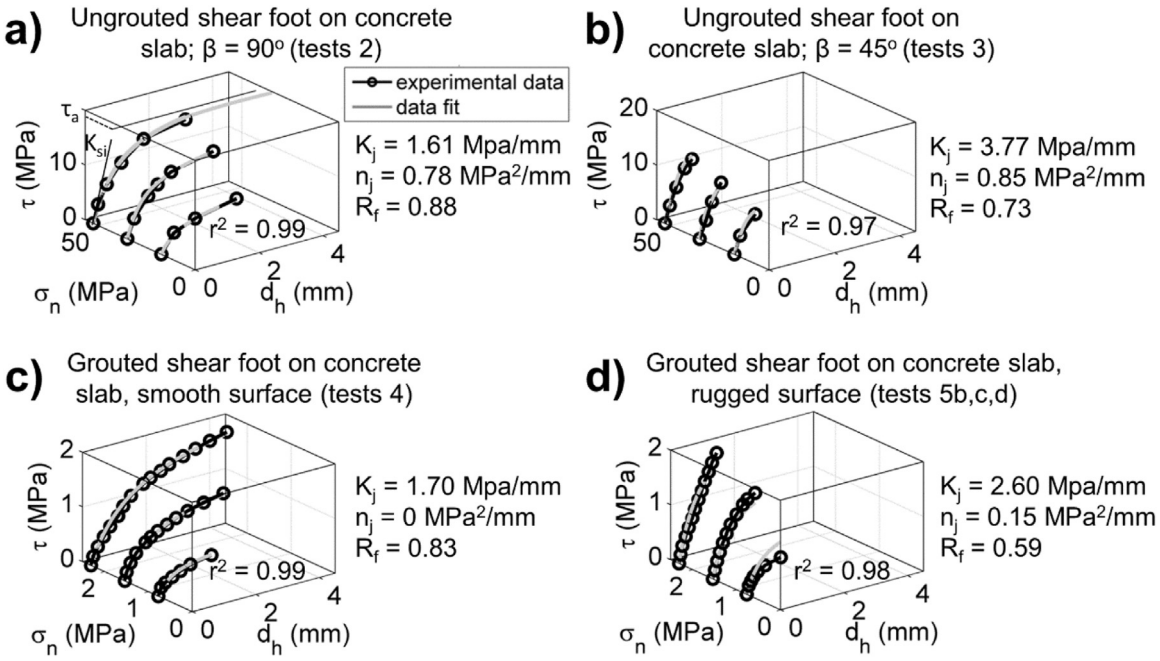

Fig. 10. Shear stress – shear displacement (τ–d_h) curves for different levels of applied normal stress σ_n. Black circles refer to experimental data; the gray lines correspond to data fitting by applying Eqs. (4)–(6). Close to each panel we report the values of K_j, n_j and R_f (Eqs. (5) and (6)) that best fit the experimental data, as well as the determination coefficients r^2. Values of normal and shear stress in panels (a) and (b) differ significantly from corresponding values in (c), (d) because the area of contact shear foot-concrete slab is different, whereas applied loads and observed displacements are similar.

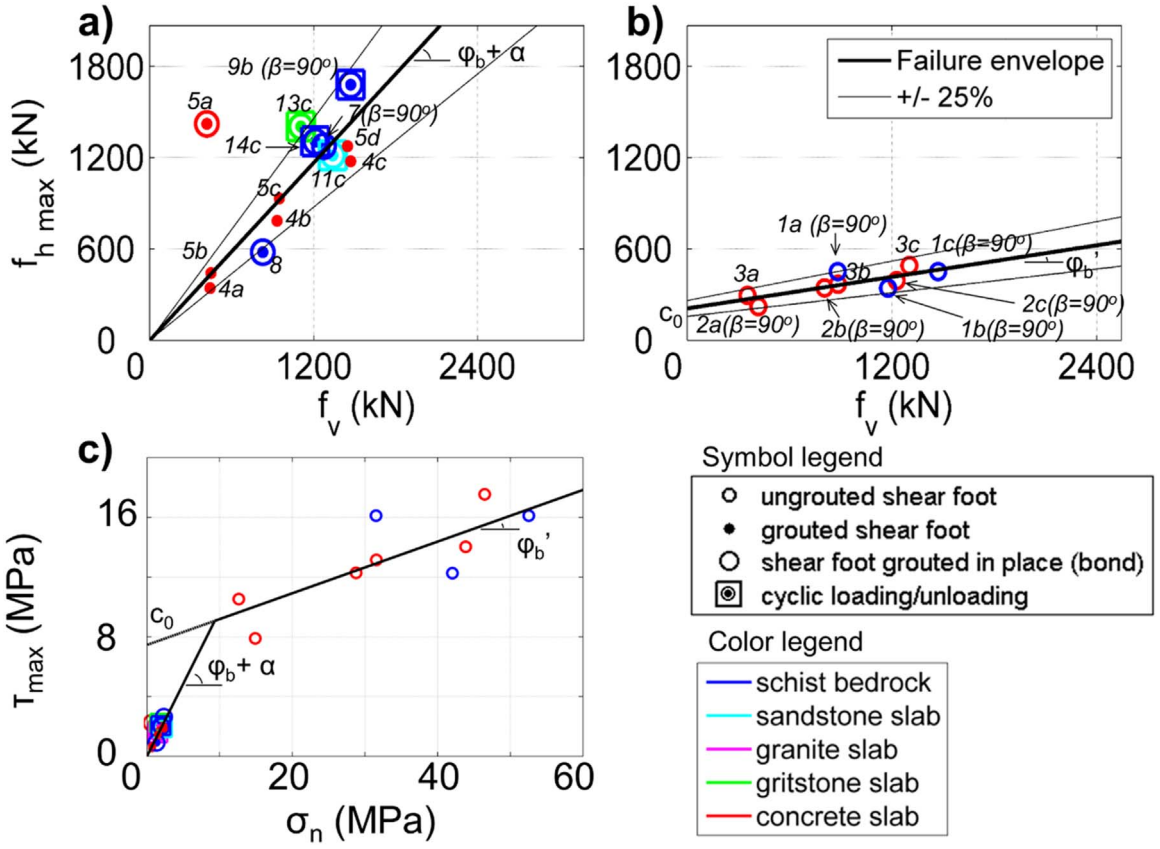

Fig. 11. Maximum shear load and vertical load at the sliding failure of the shear footing. a) Maximum shear and normal loads at sliding failure for direct shear tests with a grouted foundation footing. b) Maximum shear and normal loads at sliding failure for direct shear tests with an ungrouted foundation footing. Labels in (a) and (b) indicate the name of the test and the bevel angle if β=90°; β=45° otherwise. c) Conditions at failure from (a) and (b) expressed in terms of maximum shear and normal stresses.

compliance to a consistent failure envelope in Fig. 11a is in agreement with the experimental observation that mechanisms involved in the shear resistance of the shear foot-rock system, such as friction in rock-to-rock contact, depend little on lithology (Byerlee, 1978; De Blasio, 2011). Indeed, the performance of the footings grouted in place (circled dots in Fig. 11a), was generally better than the tests where the grout layer was added prior to the installation of the shear foot (plain dots in Fig. 11a), with the exception of test 8. The improved behavior offered by such footing configuration can be ascribed to the bond exerted by the cured grout between the foundation footing and the underlying rock surface. The bond strength improves the coupling between the foundation and the rock; consequently, the horizontal force required for shear failure is higher than the case where the grout layer is added to the footing before its installation on the rock (in this case, there is no bond, as the grout cures separately from the rock). Even though the results from cyclic tests highlighted a decrease of asperity angle during the iterative shearing process (Donohue and Bergamo, 2016.), hence potentially affecting the value of maximum horizontal load at failure, the number and type of tests reported in Fig. 11a were not significant for a reliable comparison between monotonic and cyclic tests. Additionally, previous experimental studies have shown that the value of normal stress or the shearing velocity have a greater impact on the value of shear stress at failure when compared to the influence of loading/unloading cycles preceding failure of the rock joint (Jafari et al., 2003, 2004).

As for the shear tests conducted by directly placing the ungrouted steel frame of the foundation footing on the rock or concrete surface, the horizontal loads determining sliding failure are significantly lower (compare Figs. 11a, b). Available data points can be quite well approximated with the Patton (1966) failure criterion at high normal stresses (Eq. (8)), suggesting both cohesion and frictional mechanisms control the shear resistance. The retrieved value of cohesion (209 kN, in terms of stresses c_O=7.45 MPa) is high, comparable to the cohesive strength of an average to good quality rock mass (Hoek, 2001). This can be ascribed to the penetration of the steel frame of the shear foot in the underlying concrete surface (up to 15 mm when $f_v \approx$1471 kN) for the shear tests conducted on the concrete slab (red circles in Fig. 11b). As for the tests performed on schist (blue circles), the high value of c_O is likely to be related to interlocking between the hollow steel frame of the shear foot and the rock asperities. This interlocking/penetration mechanism appears to have a limited dependency on the level of vertical stress, as witnessed by the reduced slope of the failure envelope. It is finally worth remarking that most of the values of $f_{h\,max}$ from tests where the lower edge of the footing was beveled at 45° (tests 3a, b, c), lie in the upper portion of this interval, suggesting the greater effectiveness of this configuration (as discussed in 3.1.2).

Fig. 11c shows the failure condition in Figs. 11a and b in terms of shear and normal stresses at the base of the foundation footing (τ_{max} vs σ_n). The values of normal stress are distributed over two separate intervals (0.74–2.21 and 12.63–52.54 MPa) due to the two different testing configurations of the shear foot. When the section between the steel frame of the shear foot and the rock surface is grouted, the applied vertical loads are distributed over a wide area (approx. 0.665 m^2) and consequently σ_n values are comprised in a 0.74–2.21 MPa range. Vice versa, when only the steel frame of the shear foot is in contact with the rock, the same vertical load is distributed over a much smaller area and normal stress values are considerably higher (15–52.54 MPa). Altogether, all data points appear to coherently follow Patton's (1966) failure criterion, which predicts linear behavior with null cohesion intercept at low σ_n, while at higher normal stresses the slope of the linear envelope is lower and a nonzero cohesion is present.

4. Conclusions

A series of direct shear tests were carried out at full scale with the purpose of evaluating the potential of a tensioned anchor foundation system (designed to fasten tidal turbine devices to a rock seabed) to resist substantial shear loading. In both the testing and subsequent analysis stages, we concentrated on the primary shear resistance mechanism of tensioned anchors. The resistance to horizontal displacement offered by the anchor itself, a mechanism that arises when the foundation footing – rock coupling has already failed, was not analyzed. An ad-hoc experimental apparatus, comprising the tensioned anchor foundation enclosed in a testing rig for the application of vertical and horizontal loads, was designed and installed at a test site located in a schist quarry. The tests performed comprised a variety of different configurations for the foundation-rock system, different types of rock (from weathered schist to compact rock or concrete slabs), and various loading paths. The horizontal and vertical load-displacement datasets were studied with particular reference to i) the definition of a coherent load-displacement behavior, and ii) the definition of a failure criterion for the condition of sliding failure. For both topics of study, relationships available in the literature that were developed for the analysis of the mechanical behavior of natural rock discontinuities were used and generally showed a good agreement with our experimental data, thus validating their use for the modeling of the performance of tensioned anchor foundations. In particular, i) the shear and normal load – displacement relations can be effectively modeled with hyperbolic relations, whose mathematical parameters correlate with the arrangement of the footing-rock system and with the quality of the rock on which the foundation is installed; ii) the identified failure envelope shows either a cohesive and frictional behavior or a frictional and dilatant behavior, depending on the configuration of the base of the footing.

The key elements that improve the shear resistance of the foundation were also identified as: i) when the ungrouted steel frame of the footing is placed on the rock, a greater shear resistance is obtained by shaping the lower edge of the shear foot with a 45° angle; ii) adding a layer grout below the foundation footing significantly increases the shear performance of the foundation; iii) adding this grout layer when the footing is already in place further improves the shear resistance of the foundation. The peak shear loads at sliding failure for monotonic and cyclic tests appeared to be relatively similar; however, due to the lack of a significant number of experiments systematically comparing monotonic and cyclic loading paths before failure, it is not possible to draw any reliable conclusions on this topic. Additional tests and studies regarding this subject are needed and envisaged for the future.

Acknowledgements

The work presented in this paper was part of the “Tension Piles for Marine Renewables” project funded by the Centre for Advanced Sustainable Energy (CASE), Invest Northern Ireland.

Appendix A

See Tables A1–A5.

Table A1
Details of tests 1–3 (footing of foundation constituted by steel frame only).

Test number	Footing configuration	Material below footing	f_v at start of test (f_{vo})	f_h load path	Recorded data	Failure
Test 1a	Steel frame only; β=90°	Schist bedrock	883 kN	Monotonic load increment to max. f_h=451 kN	f_h, f_v	Yes
Test 1b	Steel frame only; β=90°	Schist bedrock	1177 kN	Monotonic load increment to max. f_h=343 kN	f_h, f_v	Yes
Test 1c	Steel frame only; β=90°	Schist bedrock	1471 kN	Monotonic load increment to max. f_h=451 kN	f_h, f_v	Yes
Test 2a	Steel frame only; β=90°	Concrete slab	490 kN	Monotonic load increment to max. f_h=221 kN	f_h, f_v, d_h	Yes
Test 2b	Steel frame only; β=90°	Concrete slab	981 kN	Monotonic load increment to max. f_h=368 kN	f_h, f_v, d_h	Yes
Test 2c	Steel frame only; β=90°	Concrete slab	1471 kN	Monotonic load increment to max. f_h=490 kN	f_h, f_v, d_h	Yes
Test 3a	Steel frame only; β=45°	Concrete slab	490 kN	Monotonic load increment to max. f_h=294 kN	f_h, f_v, d_h	Yes
Test 3b	Steel frame only; β=45°	Concrete slab	981 kN	Monotonic load increment to max. f_h=343 kN	f_h, f_v, d_h	Yes
Test 3c	Steel frame only; β=45°	Concrete slab	1471 kN	Monotonic load increment to max. f_h=392 kN	f_h, f_v, d_h	Yes

Table A2
Details of tests 4–5 (grouted footing placed on a concrete slab).

Test number	Footing configuration	Material below footing	f_v at start of test (f_{vo})	f_h load path	Recorded data	Failure
Test 4a	Grouted footing; β=45°	Concrete slab	490 kN	Monotonic load increment to max. f_h=343 kN	f_h, f_v, d_h	Yes
Test 4b	Grouted footing; β=45°	Concrete slab	981 kN	Monotonic load increment to max. f_h=784 kN	f_h, f_v, d_h	Yes
Test 4c	Grouted footing; β=45°	Concrete slab	1471 kN	Monotonic load increment to max. f_h=1177 kN	f_h, f_v, d_h	Yes
Test 5a	Footing grouted in place; β=45°	Concrete slab	490 kN	Monotonic load increment to max. f_h=1422 kN	f_h, f_v, d_h	Yes
Test 5b	Grouted footing; β=45°	Concrete slab	490 kN	Monotonic load increment to max. f_h=441 kN	f_h, f_v, d_h	Yes
Test 5c	Grouted footing; β=45°	Concrete slab	981 kN	Monotonic load increment to max. f_h=932 kN	f_h, f_v, d_h	Yes
Test 5d	Grouted footing; β=45°	Concrete slab	1471 kN	Monotonic load increment to max. f_h=1275 kN	f_h, f_v, d_h	Yes

Table A3
Details of tests 6–10 (grouted footing placed on schist bedrock).

Test number	Footing configuration	Material below footing	f_v at start of test (f_{vo})	f_h load path	Recorded data	Failure
Test 6	Grouted footing; β=45°	Schist bedrock	1471 kN	9 unidirectional cycles max. f_h=490 kN	f_h, f_v, d_h	No
Test 7	Footing grouted in place; β=45°	Schist bedrock	1471 kN	Monotonic load increment to max. f_h=1030 kN	f_h, f_v	Yes
Test 8	Footing grouted in place; β=90°	Schist bedrock	1422 kN	Monotonic load increment to max. f_h=1275 kN	f_h, f_v d_h	Yes
Test 9a	Footing grouted in place; β=90°	Schist bedrock	1471 kN	5 unidirectional cycles max. f_h=490	f_h, f_v d_h	No
Test 9b	Footing grouted in place; β=90°	Schist bedrock	1471 kN	Monotonic load increment to max. f_h=1680 kN	f_h, f_v d_h	Yes
Test 10a	Footing grouted in place; β=45°	Schist bedrock	1471 kN	5 bidirectional loading cycles, max. $\|f_h\|$=735 kN	f_h, f_v d_h, d_v	No
Test 10b	Footing grouted in place; β=45°	Schist bedrock	1471 kN	3 bidirectional loading cycles, max. $\|f_h\|$=981 kN	f_h, f_v d_h, d_v	No
Test 10c	Footing grouted in place; β=45°	Schist bedrock	1471 kN	3 bidirectional loading cycles, max. $\|f_h\|$= 981–1716 kN	f_h, f_v d_h, d_v	No

Table A4
Details of tests 11–13 (grouted footing placed various rock materials).

Test number	Footing configuration	Material below footing	f_v at start of test (f_{vo})	f_h load path	Recorded data	Failure
Test 11a	Footing grouted in place; β=45°	Sandstone slab	1471 kN	5 bidirectional loading cycles, max. $\|f_h\|$=735 kN	f_h, f_v d_h, d_v	No
Test 11b	Footing grouted in place; β=45°	Sandstone slab	1471 kN	2 bidirectional loading cycles, max. $\|f_h\|$=981 kN	f_h, f_v d_h, d_v	No
Test 11c	Footing grouted in place; β=45°	Sandstone slab	1471 kN	4 bidirectional loading cycles, max. $\|f_h\|$=1177–1216 kN	f_h, f_v d_h, d_v	Yes
Test 12a	Footing grouted in place; β=45°	Granite slab	1471 kN	5 bidirectional loading cycles, max. $\|f_h\|$=735 kN	f_h, f_v d_h, d_v	No
Test 12b	Footing grouted in place; β=45°	Granite slab	1471 kN	2 bidirectional loading cycles, max. $\|f_h\|$=981 kN	f_h, f_v d_h, d_v	No
Test 13a	Footing grouted in place; β=45°	Gristone slab	1471 kN	5 bidirectional loading cycles, max. $\|f_h\|$=735 kN	f_h, f_v d_h, d_v	No
Test 13b	Footing grouted in place; β=45°	Gristone slab	1471 kN	3 bidirectional loading cycles, max. $\|f_h\|$=981 kN	f_h, f_v d_h, d_v	No
Test 13c	Footing grouted in place; β=45°	Gristone slab	1471 kN	4 bidirectional loading cycles, max. $\|f_h\|$=1177–1667 kN	f_h, f_v d_h, d_v	Yes

Table A5
Details of test 14 (long term, cyclic loading tests on schist bedrock).

Test number	Footing configuration	Material below footing	f_v at start of test (f_{vo})	f_h load path	Recorded data	Failure
Test 14a	Footing grouted in place; β=45°	Schist bedrock	1471 kN	48 bidirectional loading cycles, max. $\lvert f_h \rvert$ =490 kN	f_h, f_v d_h,d_v	No
Test 14b	Footing grouted in place; β=45°	Schist bedrock	1471 kN	46 bidirectional loading cycles, | max. $\lvert f_h \rvert$ =735 kN	f_h, f_v d_h,d_v	No
Test 14c	Footing grouted in place; β=45°	Schist bedrock	1471 kN	8 bidirectional loading cycles, max. $\lvert f_h \rvert$ =981–1471 kN	f_h, f_v d_h,d_v	Yes

References

Abhinav, K.A., Saha, N., 2015. Coupled hydrodynamic and geotechnical analysis of jacket offshore wind turbine. Soil Dyn. Earthq. Eng. 73, 66–79.

Adhikari, S., Bhattacharya, S., 2011. Vibrations of wind turbines considering soil structure interaction. Wind Struct. 15 (2), 85–112.

Alejano, L.R., Alonso, E., 2005. Considerations of the dilatancy angle in rocks and rock masses. Int. J. Rock Mech. Min. Sci. 42, 481–507.

Bandis, S.C., 1980. Experimental Studies of Scale Effects on Shear Strength and Deformation of Rock Joints (Ph.D. thesis). University of Leeds, UK.

Bandis, S.C., Lumsden, A.C., Barton, N.R., 1983. Fundamentals of rock joint deformation. Int. J. Rock Mech. Min. Sci. Geomech. Abstr. 20 (6), (249 268).

Barton, N., 1973. Review of a new shear strength criterion for rock joints. Q. J. Eng. Geol. 7, 287–332.

Bhattacharya, S., Cox, J.A., Lombardi, D., Wood, D.M., 2012. Dynamics of offshore wind turbines supported on two foundations. Geotech. Eng. 166 (GE2), 159–169.

de Blasio, F.V., 2011. Introduction to the Physics of Landslide. Springer Publishing, New York.

BS EN 14199, 2015. Execution of Special Geotechnical Works – Micropiles. BSI, London.

BS EN 14490, 2010. Execution of Special Geotechnical Works - Soil Nailing. BSI, London.

Byerlee, J., 1978. Friction of rocks. Pure Appl. Geophys. 116 (4), 615–626.

Byrne, B.W., Houlsby, 2003. Foundations for offshore wind turbines. Philos. Trans. R. Soc. Lond. A 361, 2909–2930.

Callan, D., McCarey J., Holland A., 2012. A System and Method for the Installation of Underwater Foundations. Patent No. WO/2012/123431.

Donohue, S., Bergamo, P., 2016. Assessing the full-scale performance of tension pile foundations under monotonic and cyclic shearing using direct shear tests. In: Proceedings of the 2nd International Conference on Offshore Renewable Energy (CORE 2016), ASRANet, Glasgow, UK.

EMEC, 2016. the European Marine Energy Centre Ltd. ⟨http://www.emec.org.uk/⟩ (accessed 15.01.16.).

Eurocode 7, BS EN 1997, 1997. Eurocode 7: Geotechnical Design. BSI, London.

European Committee for Standardization, 2000. EN 206-1 Concrete - Part 1: Specification, Performance, Production and Conformity. CEN, Brussels.

Gu, X.F., Haberfield, C.M., 2004. Laboratory investigation of shaft resistance for piles socketed in Basalt. Int. J. Rock Mech. Min. Sci. 41 (3), 465.

Hoek, E., 2001. Rock mass properties in underground mines. In: Hustrulid, W.A., Bullock, R.L. (Eds.), Underground Mining Methods: Engineering Fundamentals and International Case Studies. Society for Mining, Metallurgy, and Exploration (SME), Litleton, Colorado.

Hoek, E., Brown, E.T., 1980. Empirical strength criterion for rock masses. J. Geotech. Eng. Div. 106 (GT9), 1013–1035.

Huang, X., Haimson, B.C., Plesha, M.E., Qiu, X., 1993. An investigation of the mechanics of rock joints – Part I laboratory investigation. Int. J. Rock Mech. Min. Sci. Geomech. Abstr. 30 (3), 257–269.

Hungr, O., Coates, D.F., 1978. Deformability of joints and its relation to rock foundation settlements. Can. Geotech. J. 15, 239–249.

IEA – RETD, 2012. International Energy Authority Renewable Energy Technology Deployment: Offshore Renewable Energy. Routledge, London.

Ischebeck Titan, 2016. ⟨http://www.ischebecknz.co.nz/pdf/Injection%20Piles.pdf⟩ (accessed 19.01.16.).

Jaeger, J.C., 1971. Friction of rocks and stability of rock slopes. Geotechnique 21 (2), 97–134.

Jafari, M.K., Pellet, F., Boulon, M., Amini Hosseini, K., 2004. Experimental study of mechanical behaviour of rock joints under cyclic loading. Rock Mech. Rock Eng. 37 (1), 3–23.

Jafari, M.K., Hosseini, K.A., Peller, F., Boulon, M., Buzzi, O., 2003. Evaluation of the shear strength of rock joints subjected to cyclic loading. Soil Dyn. Earthq. Eng. 23, 619–630.

Jeffcoate, P., Starzmann, R., Elsaesser, B., Scholl, S., Bischoff, S., 2015. Field measurements of a full scale tidal turbine. Int. J. Mar. Energy 12, 3–20.

de Jesus Henriques, T.A., Tedds, S.C., Botsari, A., Najafian, G., Hedges, T.S., Sutcliffe, C.J., Owen, I., Poole, R.J., 2014. The effects of wave-current interaction on the performance of a model horizontal axis turbine. Int. J. Mar. Energy 8, 17–35.

Johnston, I.W., Lam, 1989. Shear behaviour of regular triangular concrete/rock joints – analysis. J. Geotech. Eng. 115 (5), 711–727.

Kulhawy, F.H., 1975. Stress deformation properties of rock and rock discontinuities. Eng. Geol. 9, 327–350.

Kulhawy, F.H., 1978. Geomechanical model for rock foundation settlement. J. Geotech. Eng. Div. 104 (GT2), 211–225.

McLaughlin, Harvey, 2016. ⟨https://www.mclh.co.uk/projects/openhydro-450t-gravity-base-installation-bay-of-fundy-canada/⟩ (accessed 19.01.16.).

Meggitt, D.J., Jackson, E., Machin, J., Taylor, R., 2013. Marine micropile anchor systems for marine renewable energy applications. In: Proceedings of the Oceans Conference, SanDiego, pp.1–7.

Patton, F.D., 1966. Multiple modes of shear failure in rocks. In: Proceedings of First Congress of International Society of Rock Mechanics, vol. 1, pp. 509–513.

Qiu, X., Plesha, M.E., 1991. A theory for dry wear based on energy. J. Tribol. 113, 442–451.

Renewable UK, 2013. Wave and Tidal Energy in the UK. Renewable UK, London.

Roosta, R.M., Sadaghiani, M.H., Pak, A., Saleh, Y., 2006. Rock joint modelling using visco-plastic multilaminate model at constant normal load condition. Geotech. Geol. Eng. 24, 1449–1468.

Scotenewables, 2016. ⟨http://www.scotrenewables.com/⟩ (accessed 19.01.16.).

Serrano, A., Olalla, C., 2004. Shaft resistance of a pile embedded in rock. Int. J. Rock Mech. Min. Sci. 41, 21–35.

Serrano, A., Olalla, C., 2006. Shaft resistance piles in rock: comparison between in situ test data and theory using the Hoek and Brown failure criterion. Int. J. Rock Mech. Min. Sci. 43, 826–830.

Spagnoli, G., Weixler, L., Stefan, Finkenzeller, 2013. Drilling tools for installation of offshore wind foundations. Sea Technol. 54 (1), 47–49.

DETINI, Department of Enterprise, Trade and Investment of Northern Ireland, 2009. Offshore Renewable Energy Strategic Action Plan. Department of Enterprise, Trade and Investment, Belfast, 2012–2020.

Tiwari, P., Chandak, R., Yadav, R.K., 2014. Effect of salt water on compressive stength of concrete. J. Eng. Res. Appl. 4 (4), 38–42.

UK Government, 2003. Energy White Paper: Our Energy Future - Creating a Low Carbon Economy. Department of Trade and Industry, (available at)⟨http://webarchive.nationalarchives.gov.uk/+/http:/www.berr.gov.uk/files/file10719.pdf⟩.

Whittaker, T., Collier D., Folley M., Henry A., Crowley M., 2007. The development of oyster-a shallow water surging energy converter. In: Proceedings of the 7th European Wave and Tidal Energy Conference, Porto, Portugal, 2007.